



## Activated carbons developed from Algerian agro-waste of palm trunk fiber: characterization and adsorptive capacity for azo dyes removal

Firouz Cherdoud<sup>a,b</sup>, Selma Khelifi<sup>c,d,\*</sup>, Abdelbaki Reffas<sup>b</sup>

<sup>a</sup>Environment and Durable Development Laboratory, University of M'sila, M'sila 28000, Algeria, email: firouz.cherdoud@univ-msila.dz

<sup>b</sup>Inorganic Materials Laboratory, Department of Chemistry, Faculty of Sciences, University of Mohamed Boudiaf, M'sila 28000, Algeria, email: abdelbaki.reffas@univ-msila.dz

<sup>c</sup>Laboratoire des Applications de la Chimie aux Ressources et Substances Naturelles et à l'Environnement (LACReSNE), Université de Carthage, Faculté de Sciences de Bizerte, Zarzouna 7021, Tunisia, email: selma.khelifi@gmail.com

<sup>d</sup>Université de Tunis, 92, Boulevard 9 Avril 1938-1007, Tunis

Received 19 April 2023; Accepted 11 September 2023

### ABSTRACT

In this work, the activated carbon of palm trunk fiber was prepared by the thermochemical activation method for the adsorptive removal of azo dyes known for their toxicity, including methylene blue (MB) and methyl orange (MO) from aqueous solution. This preparation was realized with activated factor phosphoric acid  $H_3PO_4$  at 450°C in different impregnation ratios, which varied within the following range: 30, 60, 100, and 150 wt.%. Investigated adsorbents were characterized using several methods such as X-ray diffraction,  $N_2$  sorption, Fourier-transform infrared spectroscopy, energy-dispersive X-ray spectroscopy, thermogravimetric analysis, and scanning electron microscopy techniques. Also, Boehm titrations and point of zero charge measurements were carried out to give more explication about surface properties. The effect of adsorbent dosage was evaluated and discussed. The results show that the adsorption capacity increases with increasing the mesoporous of the activated carbons. At 150 wt.%  $H_3PO_4$  ratios were found to be appropriate for efficient adsorption of the (MO) dye ( $\sim 862 \text{ mg}\cdot\text{g}^{-1}$ ) and (MB) dye ( $\sim 508 \text{ mg}\cdot\text{g}^{-1}$ ). Isotherm data were investigated according to Langmuir and Freundlich equations. The obtained results revealed that the Langmuir model provides the best fit for the cationic MB dye while the Langmuir and Freundlich models offer the best fit for anionic MO dye.

*Keywords:* Activated carbons; Characterized; Adsorptive removal; Palm trunk fiber; Langmuir and Freundlich models; Azo dyes

### 1. Introduction

For a good life, we need a clean environment with crucial measures for protecting water, soil, and the atmosphere. Today, with the progression of analytical methods an increase in ground and wastewater pollution has been noted by various organic and inorganic compounds. Currently, agricultural and industrial sources are the primary sources of these toxins and pollutants, which include heavy metals, plasticizers, pesticides, pharmaceutical residues, and dyes.

Among them, textile dyes are frequently used in industrial applications such as textile, leather, and dye manufacturing [1]. The colored effluents of wastewater from these industries can be transferred to drinking water bringing a threat to human health due to their toxic and carcinogenic effects [2].

In effect, dyes usually have complex aromatic molecular structures which make them more difficult to biodegrade and treat. Therefore, it is necessary to treat these pollutants [2]. Numerous physicochemical methods and

\* Corresponding author.

traditional techniques have been used to treat and remove dyes from wastewater such as biological degradation [3], electrochemical removal [4], sedimentation [5], ion exchange [6], photodegradation [7,8], and adsorption. These methods are expensive, need more time for treatment, and high energy. Different studies have shown that adsorption phenomena are significant for pollutant removal [9]. Adsorption is regarded as an effective technique independent of the nature of the adsorbate. Activated carbon is the most commonly used adsorbent owing to its large surface area and microporous structure, high surface reactivity, and low cost, which adsorb pollutant molecules through chemical or physical interactions [10]. Those adsorbents are from materials such as precursors rich in carbon through the carbonization process and activation. Generally, porous carbon synthesis depends on the activation procedure and nature of raw materials [11]. Carbonization and activation steps are reached simultaneously in the chemical activation process [12]. It has many advantages compared to physical activation, such as short processing time, low activation temperature, high yield, and high development of the mesoporous surface area [13]. The raw material is impregnated with an activating reagent and heated under an inert atmosphere, that is,  $H_3PO_4$  [14],  $HCl$  [15],  $ZnCl_2$  [16]. In addition, phosphoric acid is commonly used in the preparation of carbon adsorbent with lignocellulosic materials giving the possibility to develop microporous and/or mesoporous carbon with a specific surface area depending on the temperature of activation [16].

This study focuses on activated carbon synthesis from palm trunk fibers as an agricultural byproduct precursor because of its availability in Algeria [17,18]. It is not exploited since it is not employed commercially. For this aim, phosphoric acid is used as a dehydrating agent in a chemical activation process. The physical and chemical properties were studied for the determination of adsorption properties. In addition, the objective of this study is to evaluate the performance of activated carbons that adsorb methylene blue (MB) and methyl orange (MO) dyes from aqueous

solutions. Also, to further explain the experimental results, adsorption isotherms are investigated.

## 2. Experimental section

### 2.1. Materials and products

#### 2.1.1. Adsorbates and other chemicals

All chemicals used in this work were of analytical grade. Model pollutants are anionic azo dye: methyl orange (MO) and cationic dye: methylene blue (MB). The main properties of these studied dyes are reported in Table 1.

### 2.2. Preparation of the investigated adsorbents

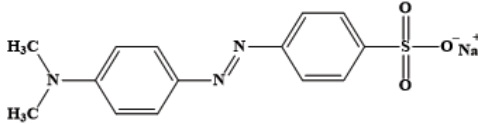
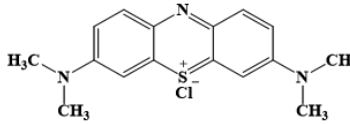
#### 2.2.1. Agro-waste of palm trunk fiber

The agro-waste used in this study namely palm trunk fibers (Fig. 1), is collected from the El-Oued region situated in the northeast of Algeria ( $33^{\circ}22'6''N$ ,  $6^{\circ}52'3''E$ ). Before using this agro-waste, the diameter of the fibers was



Fig. 1. Visual aspect of a palm trunk fiber.

Table 1  
Properties of methyl orange and methylene blue

Parameters	Value	
Name	Methyl orange	Methylene blue
Molecular formula	$C_{14}H_{14}N_3O_3SNa$	$C_{16}H_{18}N_3SCl$
Molecular weight ( $g \cdot mol^{-1}$ )	327.33	319.85
$\lambda_{max}$ (nm)	464	664
Chemical structure		
3D structure		

reduced to 800  $\mu\text{m}$  and it was washed with distilled water to remove impurities. The obtained product is dried at 50°C for 48 h to reduce the moisture content and then sieved for regular diameter.

### 2.2.2. Synthesis of activated carbons

The palm trunk fibers were impregnated with a weight amount (calculated from the density multiplied by the volume and the percentage) of  $\text{H}_3\text{PO}_4$  aqueous solution and then heat-treated at 450°C in an air atmosphere. With a different impregnation ratio ( $X_p$ , in wt.%) of 30, 60, 100, and 150 wt.%, namely PAC30%, PAC60%, PAC100%, and PAC150%, respectively (prepared activated carbons wt.%). To obtain activated carbons of variable porosity,  $X_p$  was defined as the ratio percentage and it was calculated via Eq. (1):

$$\% = \left[ \frac{\text{the weight of } \text{H}_3\text{PO}_4 \text{ (g)}}{\text{the weight of precursor (g)}} \right] \times 100 \quad (1)$$

The palm trunk fibers were impregnated for 24 h with phosphoric acid solutions (100 mL) to form slurries and then dried at 110°C for 24 h. Samples were calcined for 1 h at 450°C (heating rate 10°C·min<sup>-1</sup>). The residual phosphoric acid has been eliminated from samples by washing with boiled distilled water until no phosphate ions have been detected in the water. Fig. 2 shows the preparation method; so that the wash water of samples was analyzed by pH meter to confirm the absence of residual phosphate particles by measuring the pH until proven at 6. After drying at 110°C for 5 h, the final material was crushed and sieved to obtain particles with a diameter < 80  $\mu\text{m}$ . The yield of prepared activated carbon was calculated via Eq. (2):

$$\text{yield}(\%) = \left( \frac{W_1}{W_0} \right) \times 100 \quad (2)$$

where  $W_1$ : the activated carbon mass after activation,  $W_0$ : the mass of the precursor.

The “burn-off” is the weight loss percentage due to the activation step indicated in Eq. (3):

$$\text{burn-off}(\%) = 100 - \text{yield}\% \quad (3)$$

### 2.2.3. Characterization of the synthesized prepared activated carbons

The specific surface area, pore volume, and pore size distribution are determined from  $\text{N}_2$  adsorption over the relative pressure  $P/P_0 = 0.99$  at a liquid nitrogen temperature of 196°C. All samples were degassed at 300°C for 12 h under vacuum then the microporous volume was determined by the  $t$ -plot method [19]. The Brunauer–Emmett–Teller (BET) equation was used to calculate the specific surface areas ( $S_{\text{BET}}$ ) of the activated carbons with the area of the nitrogen molecule assumed at 0.162 nm<sup>2</sup>. The microporous surface and the external surface area were calculated from the  $t$ -plot. The total pore volumes were estimated as the liquid volume of adsorbed adsorbate  $\text{N}_2$ . Furthermore, the pore size distribution was calculated using the Barrett–Joyner–Halenda (BJH) method on the adsorption/desorption hysteresis loop, assuming a cylindrical open-ended pore model [20].

Scanning electron microscopy (SEM) was used to bring insights into the structure of investigated adsorbents and to visualize their morphologies. Also, powder X-ray diffraction patterns of the samples were observed by diffractometer (PANalytical X'pert HighScore Plus Diffractometer, Malvern). Energy-dispersive X-ray spectroscopy (EDX) coupled with SEM was used to determine the chemical composition of all materials.

The  $\text{pH}_{\text{PZC}}$  was resolved by the so-called pH drift method [21], it is a property that determines the pH at which the surface exhibits net electrical neutrality. The pH of the suspension of 0.15 mg activated carbon and 50 mL NaCl aqueous solution at 0.01 M was adjusted to successive initial

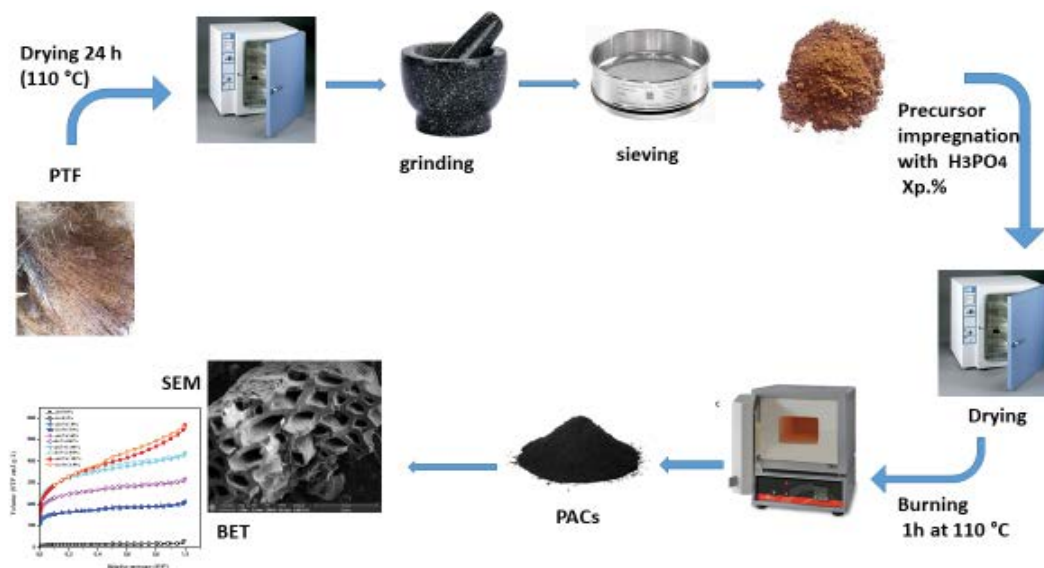


Fig. 2. Illustration of the method for preparing activated carbons with phosphoric acid activation of different prepared activated carbons.

values between 2 and 12. The suspensions were stirred for 48 h and the final pH was measured and plotted vs. the initial pH. The  $\text{pH}_{\text{PZC}}$  is determined at the value for which  $\text{pH}_{\text{final}} = \text{pH}_{\text{initial}}$  [22].

The thermogravimetric analysis (Shimadzu TGA-51, Kyoto, Japan) was used to detect the effect of the phosphoric acid impregnation ratio used for the thermochemical activation on the mass loss (burn-off) studies of the materials. About (200 mg) of the sample was heated from 25°C to 800°C with a heating rate of 10°C min<sup>-1</sup>.

Fourier-transform infrared spectroscopy (FTIR-Shimadzu 8300, in the range 4,000–400 cm<sup>-1</sup> using KBr pellets) was used to determine the functional groups on the surface of samples.

The method of selective neutralization or Boehm titration consists of neutralizing the oxygen groups according to their acid strength on activated carbon [23] and estimating the number of bases within the material [24]. Experimentally, about 0.15 g of each sample prepared activated carbons (PACs) was mixed in a closed flask with 50 mL of a 0.1 M aqueous reactant solution (NaOH, Na<sub>2</sub>CO<sub>3</sub>, NaHCO<sub>3</sub>, or HCl). The mixtures were stirred for 48 h at a constant speed of 300 rpm at ambient temperature then the suspensions were filtrated. To determine the oxygenated group contents, the back-titrations of the filtrate 20 mL were achieved with HCl 0.1 M. The basic group contents were also determined by back titration of the filtrate with NaOH 0.1 M.

#### 2.2.4. Batch adsorption experiments

The adsorption experiments were executed with 10 mg of PACs samples placed in 100 mL, glass bottles containing 25 mL of dye solution at various concentrations in the range of 5–1,000 mg·L<sup>-1</sup>. The pH of the dye solutions was adjusted at pH = 6 by hydrochloric acid 1 and 0.1 mol·L<sup>-1</sup> or sodium hydroxide 1 and 0.1 mol·L<sup>-1</sup> solution. The adsorption equilibrium of MB on materials was achieved for 24 h of stirring at 25°C ± 1°C and 300 rpm. Subsequently, the samples were centrifuged at 1,500 rpm for 20 min to separate the adsorbents from the aqueous solutions depending on the case. The MB equilibrium concentrations of the samples were analyzed by spectrophotometer (Shimadzu UV-2101PC) at 665 nm.

The adsorption of the anionic dye methyl orange (MO), also were realized in batch adsorption experiments. The adsorption isotherms of MO were studied at pH = 4 for 24 h at 25°C ± 1°C. Adsorption experiments were carried out with the same procedure as the previous MB dye. After adsorption equilibrium, suspensions were centrifuged at 1,500 rpm for 20 min, and then analyzed by UV-Visible spectroscopy at 464 nm to determine the residual equilibrium dye concentration ( $C_e$ ). The amount of equilibrium adsorption MB and MO adsorbed on activated carbons ( $q_e$  in mg·g<sup>-1</sup>) was evaluated using Eq. (4):

$$q_e = \frac{(C_0 - C_e)V}{m} \quad (4)$$

where  $C_e$  (mg·L<sup>-1</sup>) is the liquid concentration of the dye at equilibrium,  $C_0$  (mg·L<sup>-1</sup>) is the initial concentration of the dye in solution,  $V$  is the volume of the solution (L), and  $m$

is the mass of the adsorbent (g). Adsorption isotherms at 25°C of the dyes MB and MO on the activated carbon samples PACs were analyzed using Langmuir, Freundlich, and Temkin isotherms, respectively in Eqs. (5)–(7) [25,26]:

$$q_e = \frac{q_m(K_L C_e)}{(1 + K_L C_e)} \quad (5)$$

$$q_e = K_F C_e^{1/n} \quad (6)$$

$$q_e = B \ln(A_T C_e) \quad (7)$$

where  $C_e$  and  $q_e$  are respectively the adsorbate equilibrium concentrations in the liquid and solid phases,  $q_m$  is the maximum adsorption capacity according to the Langmuir model,  $K_L$ ,  $K_F$ , and  $n$ ,  $A_T$  (L·mg<sup>-1</sup>) are constants, where  $K_T$  is the constant related to the variation of adsorption energy (J·mol<sup>-1</sup>),  $R$  is the universal gas constant (8.314 J·mol<sup>-1</sup>·K<sup>-1</sup>) and  $T$  is the absolute temperature (K).

The model equations can be linearized, leading as indicated in Eqs. (8)–(10) [27–29]:

$$\frac{C_e}{q_e} = \left( \frac{1}{K_L q_m} \right) + \left( \frac{C_e}{q_m} \right) \quad (8)$$

$$\log q_e = \log K_F + \frac{1}{n} \log C_e \quad (9)$$

$$q_e = \left( \frac{RT}{K_T} \right) \ln A_T + \left( \frac{RT}{K_T} \right) \ln C_e \quad (10)$$

In addition, fitted to experimental data, the corresponding parameters in Tables 6 and 7 as well as the standard deviations associated with the linear fits. The maximum amount of adsorbed MB allows for estimating the sample-specific surface area covered by the MB molecule ( $S_{\text{MB}}$ ) for Eq. (11):

$$S_{\text{MB}} = q_m \times A_m \times 6.02 \times \left( \frac{10^{23}}{M_{\text{MB}}} \right) \quad (11)$$

With a molecular surface of MB ( $A_m$ ) of 1.30 nm<sup>2</sup> and the 319.85 g·mol<sup>-1</sup> molecular mass of MB ( $M_{\text{MB}}$ ).

## 3. Results and discussions

### 3.1. Characterization of the adsorbents

#### 3.1.1. X-ray diffraction

To determine the effect of the thermochemical activation with phosphoric acid at 450°C, the presence of metal impurities led to a purely amorphous carbonaceous phase or graphitization also occurred. Precursor palm trunk fiber was analyzed by X-ray diffraction (XRD), which is a fundamental method for evaluating the carbon staking structure [30]. Fig. 3 shows the obtained diffractometer. The XRD profile of the activated carbons has a few sharp and narrow peaks of high intensity. The activated carbons show

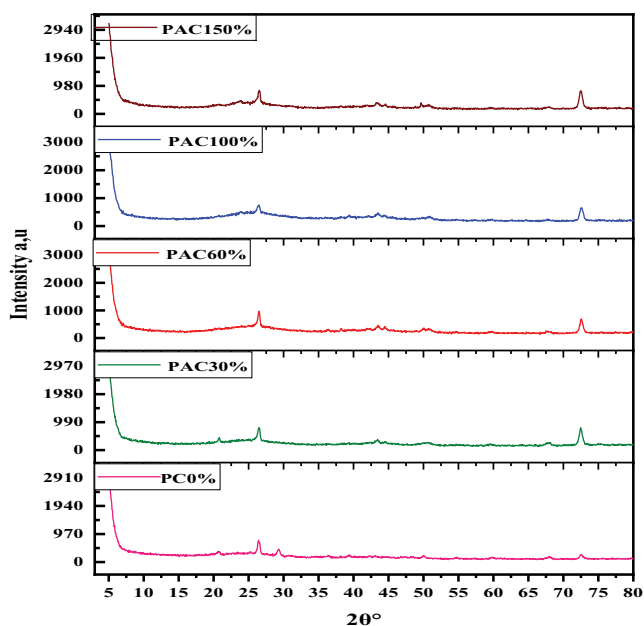


Fig. 3. X-ray diffraction patterns based on variations in the  $H_3PO_4$  ratio of PC0 and activated carbons, PAC30, PAC60, PAC100, and PAC150.

diffraction profiles of wide and sharp crests that indicate an amorphous structure, which is a valuable property for a highly porous material. The PC0 amorphous structure contributed to the high content of hemicellulose and lignin [31]. The reduction of the amorphous structure was observed for the conversion of PC0 to bio-PACs due to hemicellulose and lignin exposure to high temperatures [32]. It can be contemplated that the pattern of the sample exhibits two broad peaks of low intensity at  $2\theta$  ranging from  $17^\circ$  to  $30^\circ$  and  $38^\circ$  to  $46^\circ$ . These peaks correspond to the characteristic reflections of the (002) and (100) planes in the case of graphitized carbonaceous materials [33–35]. These peaks demonstrate a partially graphitic layer structure of bio-PACs. Although, these reflections have a broad and asymmetric shape of low intensity, suggesting a mixture of different graphitic phases and amorphous (no-ordered) carbon phases, creating a mixed matrix (framework) [36]. These results reveal that a graphitic carbonaceous phase can be produced from renewable carbon sources, like biomass, even at a relatively low temperature of activation ( $450^\circ\text{C}$ ) without the use of the activating agent,  $H_3PO_4$  known to act as a catalyst for the graphitization process to obtain graphitized carbon materials [37,38]. In 1970, Debye and Scherrer were able to demonstrate by X-ray diffraction that carbon, which contains 75% to 90% carbon depending on the type, has the same structural elements as graphite, the latter being, with diamond, one of two sources of pure elemental carbon found naturally.

The existence of an additional peak at  $72^\circ$  shows the existence of another compound trace able to X-rays in the sample non-treated with phosphoric acid and the four samples of thermochemical activated carbons, in particular, the sample thermochemical activated at 150%. The oxide peak at the processing temperature of  $450^\circ\text{C}$  is in agreement with

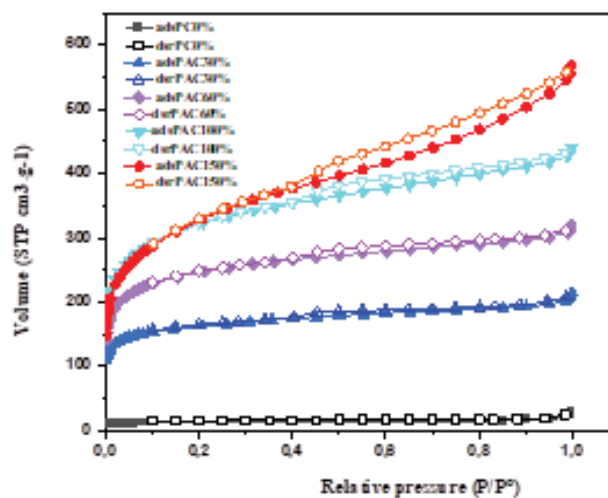


Fig. 4.  $N_2$  adsorption (full symbol)/desorption (empty symbol) isotherms at 77 K on PC0 and activated carbons, PAC30, PAC60, PAC100, and PAC150.

the EDX analysis. This peak which appeared at  $2\theta$  to  $72^\circ$  and which could be attributed to an oxide constituted the most striking result.

### 3.1.2. Specific surface area and porosity

Fig. 4 shows the nitrogen adsorption–desorption isotherms (at 77 K) of activated carbons. PAC150 and PAC100 show type IV isotherms with significant adsorption at low relative pressure ( $P/P_0$ ) and a type  $H_4$  hysteresis loop, indicating the simultaneous presence of micro/mesoporous.

According to the IUPAC technical report, these isotherms also show an  $H_4$ -type hysteresis loop characteristic of slit-shaped pores, which indicates a material that is both micro/and mesoporous [39]. Note that the loop of PAC150 is more pronounced than that of PAC100, which indicates that the mesoporous volume of PAC150 is the greatest. In addition, a substantial increase in the amount of adsorbed volume at low relative pressures in the range of  $P/P_0 < 0.02$  indicates the presence of microporous [40]. The quasi-linear part located in the 0.1–0.3 range of relative pressures is, on the other hand, an indication of the presence of mesoporous with sizes in the smallest range of mesoporous zone and/or in the super-microporous region (between 15 and  $25 \text{ \AA}$ ). Based on these characteristics, PC0 and PACs thermochemical activated are the materials that combine micro and mesoporosity. Therefore, this is affirmed by the values of the found pore volumes [40] shown in Table 2.

The PAC60 and the PAC30 isotherms are microporous material types (type I) where the filling of the microporous can occur by the primary filling at a very low relative pressure ( $P/P_0$ ) [41]. The isothermal plateaus, of PAC60 and PAC30 have been achieved. According to Table 2, the specific surface area of thermally activated carbon PC0 is  $42.32 \text{ m}^2\text{-g}^{-1}$ , after thermochemical activation by phosphoric acid, the specific surface area becomes 531.01, 809.8, 1,076.58 and  $1,130.60 \text{ m}^2\text{-g}^{-1}$ , respectively for PAC30, PAC60, PAC100, and PAC150. The surface of PC0 is relatively low

Table 2  
Textural properties obtained by adsorption/desorption studies of N<sub>2</sub> at 77 K

Carbon parameters		PC0	PAC30	PAC60	PAC100	PAC150
Total surface area (m <sup>2</sup> ·g <sup>-1</sup> )	BET <sup>a</sup>	42.32	531.01	809.84	1,076.58	1,130.60
Microporous surface area (m <sup>2</sup> ·g <sup>-1</sup> )	<i>t</i> -plot	30.19	336.26	430.93	431.84	271.78
External surface area S <sub>ext</sub> (m <sup>2</sup> ·g <sup>-1</sup> )	<i>t</i> -plot	12.13	194.74	378.91	644.73	858.82
Mesoporous surface area (m <sup>2</sup> ·g <sup>-1</sup> )	BJH <sup>b</sup> adsorption	7.64	115.01	193.93	331.38	512.21
	BJH <sup>b</sup> desorption	5.51	120.17	211.76	357.85	561.64
Total pore volume (cm <sup>3</sup> ·g <sup>-1</sup> )	Single-point adsorption <sup>c</sup>	0.027	0.303	0.466	0.646	0.810
Microporous volume (cm <sup>3</sup> ·g <sup>-1</sup> )	<i>t</i> -plot	0.014	0.166	0.214	0.212	0.129
Mesoporous volume (cm <sup>3</sup> ·g <sup>-1</sup> )	BJH <sup>b</sup> adsorption	0.021	0.115	0.179	0.296	0.558
	BJH <sup>b</sup> desorption	0.016	0.114	0.183	0.311	0.577

<sup>a</sup>Computed in the  $P/P_0$  0.25;

<sup>b</sup>BJH (Barrett–Joyner–Halenda) cumulative surface area of pores between 1.7 and 300 nm;

<sup>c</sup> $P/P_0 = 0.99$ .

compared to that of thermochemical-activated carbons. Notably, the activation of the palm fiber biomass by H<sub>3</sub>PO<sub>4</sub> with the increases in impregnation ratio brings an improvement in the specific surface area the total pore volume, and the mesoporous volumes following the destruction of the cellulose.

The values of the BET-specific surface areas of activated carbons ( $S_{BET} = 531.01$ – $1,130.60$  m<sup>2</sup>·g<sup>-1</sup>) are higher than those of others prepared from agro-residue (514–835 m<sup>2</sup>·g<sup>-1</sup>) [13]. The *t*-plot method was used to calculate the external and the microporous surface and the S<sub>ext</sub> increased strongly with the increase of the impregnation ratio. On the other hand, the microporous surface increases slightly with the increase of the ratios X<sub>p</sub> = 30%–100% and it decreases more strongly above 100% in mass. The microporous volume of the samples generally increases at the ratios while it decreases strongly at 150%. The PAC30 and PAC60, are mainly microporous and are represented by the profile of the adsorption isotherms showing that the adsorption curve coincides with the desorption curve in Fig. 4, that is, the mesoporous only represents ~37.77% and ~39.20% of the total pore volume for PAC30 and PAC60, and ~48.13% and ~71.18% for PAC100, and PAC150 shown in Fig. 5.

The pore size distribution of the BJH method Fig. 6 reveals in the activated carbon PAC150 a larger pore volume for diameters greater than 18.5 Å compared to the activated carbon PAC100. The difference between the pore size distribution of PAC100 and PAC150 lies in the presence of a larger pore volume for diameters greater than 1.9 nm and with some macroporous for PAC150. Previous works on other lignocellulosic precursors show that the amount of chemical agent (phosphoric acid) favors oxidation dehydration and plays on porosity development [42]. Jagtoyen and Derbyshire [43] explained the thermoactivation method, proposing that the dehydrating oxidizing agent H<sub>3</sub>PO<sub>4</sub> reacting within the internal cellulose structure to produce depolymerization leads to an increase in the total pore volume. In addition, those works show that when the quantity of chemical agent (H<sub>3</sub>PO<sub>4</sub>) used for the thermochemical activation increases, the volume and the content of various associated polyphosphates have increased inducing a greater pore volume and pore enlargement, promoting the formation

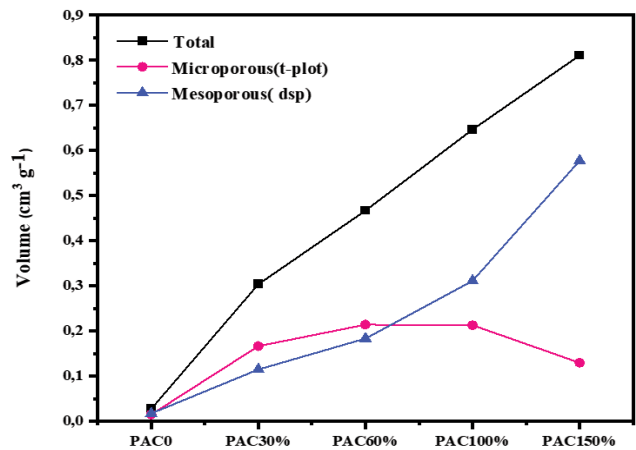


Fig. 5. Pore volume of the activated carbons (depending on X<sub>p</sub> in wt.% for the palm trunk fiber PC0 and PACs: total, microporous, and mesoporous volumes (from *t*-plot and BJH adsorption model).

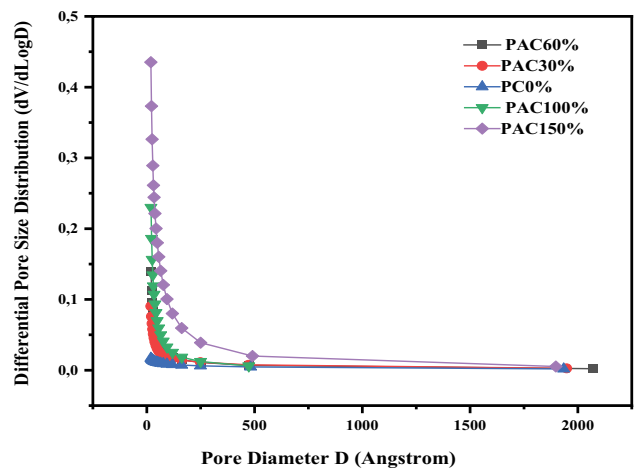


Fig. 6. Differential pore-size distribution computed from BJH of the PC0 and PACs: PAC30, PAC60, PAC100 and PAC150.

of mesoporous [43]. PAC150 possesses a high mesoporous content (~71.18%) and might be an ideal adsorbent for the removal of large molecules (organic pollutants) of size (>2 nm). A bibliographic review of phosphoric acid activation indicates that the pore size in the final activated carbon is determined by the degree of impregnation [44].

### 3.1.3. Morphology of materials and elemental analysis

Table 3 shows the energy dispersive X-ray microanalysis EDX of the PACs that contain mainly carbon (65%–86%), oxygen (28%–13%), and few amounts of nitrogen (0.29%–1.44%) and phosphorus (0.09%–0.68%) and traces of other elements for PC0, PAC150 such as Mg, Na, Al and Si originating from the wood precursor. Identified oxygen, nitrogen, and hydrogen, as significant atoms on the surface of activated carbons because of their ability to bond with other elements [45]. As the impregnation ratio increases, the carbon content increases, while the oxygen content decreases from 28% for PC0 to 13% for PAC150. The PACs contain the highest amount of carbon and oxygen and the lowest amount of heteroatoms (for example 1.44% of N). Therefore, their surface is more acidic.

The SEM micrographs of PACs produced are illustrated in Fig. 7. The surface of PC0 was a curled shape, densely packed, and porous less, and had no internal cavities caused by the presence of cellulose, hemicellulose, and lignin in raw materials without any cracks. Among the three fractions of lignocellulosic materials, lignin has been perceived as the

Table 3  
Results of the elemental analysis of PC0 and PACs (mass%)

Element (%)	PC0	PAC30	PAC60	PAC100	PAC150
C	65.69	77.32	83.37	83.11	85.29
N	0.46	0.29	1.44	1.30	0.39
O	28.26	22.00	14.41	15.21	13.52
P	0.09	0.35	0.68	0.33	0.32
S	0.19	0.05	0.09	0.04	0.05
Na	0.81	–	–	–	–
Mg	0.71	–	–	–	0.26
Al	0.47	–	–	–	–
Si	0.89	–	–	–	0.17

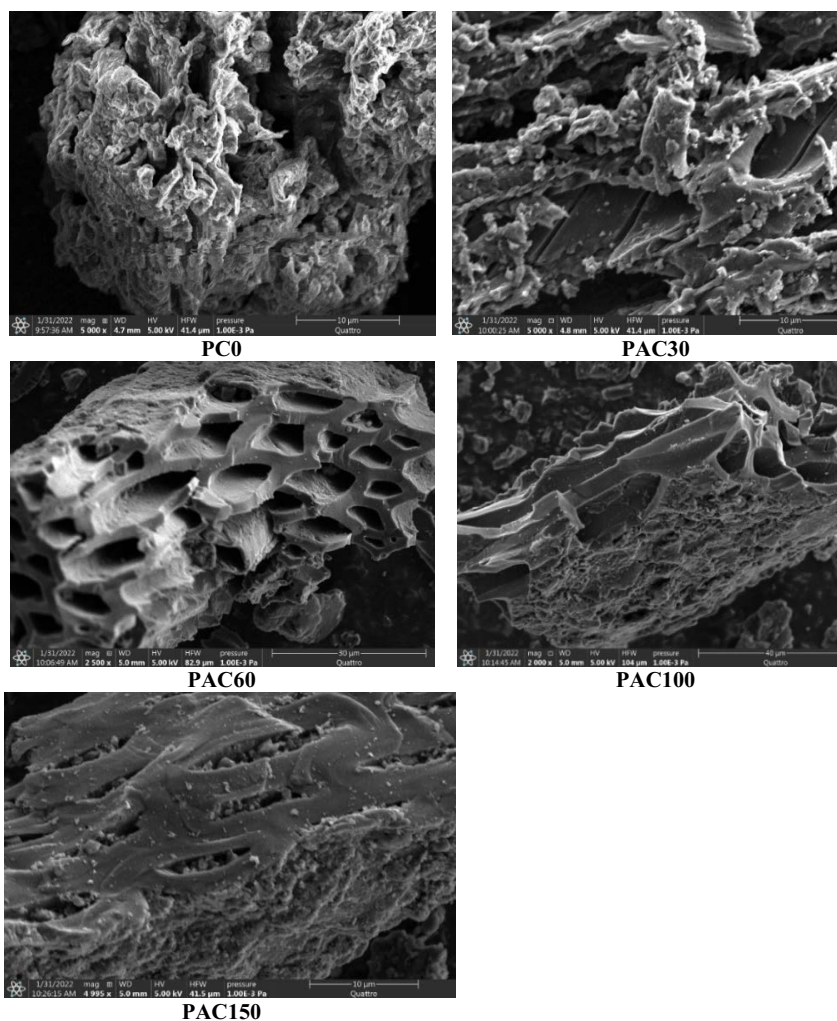


Fig. 7. Scanning electron microscopy images of the PC0, PAC30, PAC60, PAC100 and PAC150.

main component in lignocellulosic biomass responsible for the adsorption process [19]. However, as seen, the surface of PACs became rough, and some irregular pores began to form due to the removal of volatile materials following carbonization. According to the obtained BET results, as well as the change in phosphoric acid concentration with deep penetration into the carbon structure and temperature at 450°C; leads to widening pores in the activated carbon, thereby increasing its specific surface area [46] from 42.32 to 1,130.60 m<sup>2</sup>·g<sup>-1</sup>.

In the SEM images, the PACs are enlarged to the pore diameter continuously, the volume increases in the tunnel shape and overall honeycomb structure as found in the PAC60, and new pores are created due to the reaction between carbon and the activating agent as in the images shown.

3.1.4. pH<sub>PZC</sub> and surface functional groups

The pH<sub>PZC</sub> (pH of point zero charge) values are detailed in Table 4. The pH value of the prepared activated carbons decreases with an increase in the impregnation ratio, whereas the total oxygenated group contents out of results EDX obtained by selective titrations decrease. pH<sub>PZC</sub> values tend to be acidic as the ratio of phosphoric acid increases from PAC30 to PAC100. The PAC150 is a neutral carbon in agreement with its low oxygen content compared to the other prepared activated carbons, which could be attributed to the increase of the phosphoric acid impregnation ratio to a certain level, which decreases the oxygen content at the surface. The Boehm titrations of PACs, evidently show surface groups and the impregnation ratio are related. As the ratio increases from PAC30 to PAC150, the amounts of phenolic and carboxylic groups decrease, also the table shows fewer basic groups for PAC150 affirming their neutral character. The PAC30, PAC60, and PAC100 contain mainly phenolic and carboxylic groups explaining their slightly acidic characteristics.

3.1.5. Thermogravimetric analysis

The behavior of TGA curves with a heating step of PACs, as illustrated in Fig. 8, shows three steps: the first is below 150°C, and the mass loss is due to dehydration of materials such as H<sub>2</sub>O molecules physisorbed in the microporous and mesoporous. Produced from reactions, this weight loss is more than 8% for impregnation degrees PC0 and reaches 15% for PAC30 and 19% for PAC100 and PAC150.

Table 4  
Surface chemical characteristics of the activated carbons

Element (%)	PAC30	PAC60	PAC100	PAC150
Carboxylic groups (meq·g <sup>-1</sup> )	0.0075	0.0065	0.007	0.0055
Lactonic groups (meq·g <sup>-1</sup> )	0	0	0	0
Phenolic groups (meq·g <sup>-1</sup> )	0.017	0.019	0.014	0.009
Total oxygenated (meq·g <sup>-1</sup> )	0.0245	0.0255	0.021	0.0145
Total basic groups (meq·g <sup>-1</sup> )	0.091	0.089	0.094	0.09
pH <sub>PZC</sub>	5.77	5.61	5.58	7.22

The second step (250°C < T < 550°C), which corresponds to primary carbonization, shows a higher mass loss (~75%) due to the essential volatile matter and the removal of tar at 450°C, which also can be interpreted in term of a decomposition of the oxygenated surface groups. In the third step T > 550°C, the mass decrease is due to the carbonization of palm fibers, the material is almost totally carbonized (mass loss 82%–90%), which also confirms that the pyrolysis of the precursor without impregnation is not significant in term of carbon production yield. However, the mass loss plot of dried impregnated palm fibers with different impregnation ratios is shifted to higher temperatures [24].

3.1.6. IR spectroscopy

The infrared spectra measurements of PACs were performed to study the types of surface area. The spectra, illustrated in Fig. 9, show that intense bands of functional

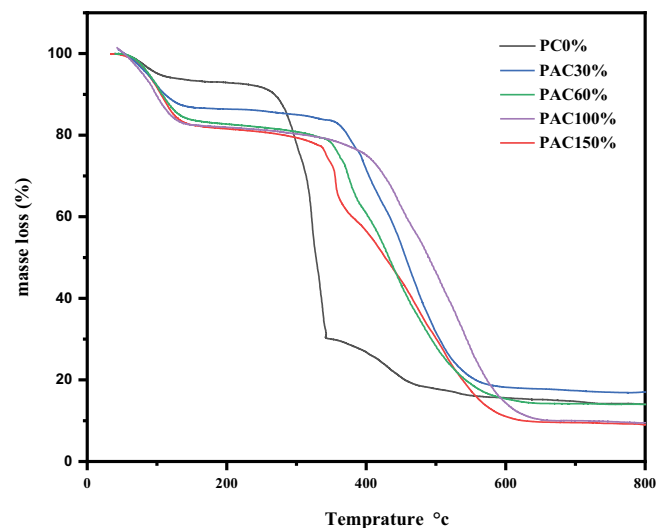


Fig. 8. Mass losses (%) vs. temperature (°C) obtained by thermogravimetric analysis for PC0, PAC30, PAC60, PAC100 and PAC150.

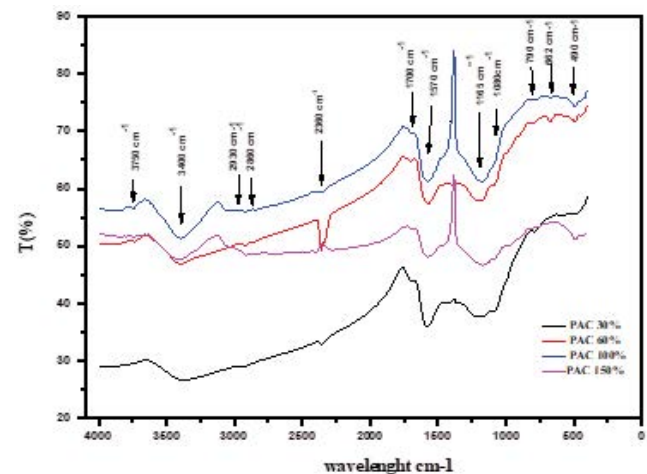


Fig. 9. Fourier-transform infrared spectra of the activated carbons: PAC30, PAC60, PAC100, and PAC150.

groups exist on the surface of the PACs. The broad absorption band at 3,100–3,600  $\text{cm}^{-1}$  at around  $\sim 3,400 \text{ cm}^{-1}$ , particularly with a large band in PAC30, was assigned to the stretching vibration of hydrogen-bonded hydroxyl groups such as (carboxyls, phenols, or alcohols), and physically adsorbed water on activated carbons. An absorption band at 3,750  $\text{cm}^{-1}$  characterizes the free O–H hydroxyl groups that appear for PAC60 and PAC100. The FTIR spectra of PACs (60, 100 and 150) show two small bands at 2,930 and 2,860  $\text{cm}^{-1}$  assigned to aliphatic C–H stretching vibrations in the aromatic methoxyl group, in methyl and methylene groups of side chains. The C–H stretching bands are detectable for the PACs prepared at a high impregnation ratio. The PACs show an absorption band at 2,360  $\text{cm}^{-1}$ , which appears more intense in the ratio of PAC60. Usually, when the small band is about 1,700  $\text{cm}^{-1}$ , assigned to C=O stretching vibrations of ketones, aldehydes, lactones, or carboxyl groups. The low intensity of the carbonyl band in this material and the absence of the characteristic band of the ketone groups suggests the presence of carboxylic and aldehydes in agreement with Boehm titrations. The peak located around 1,620 to 1,580  $\text{cm}^{-1}$  corresponds to the vibration in the plane of the aromatic rings C=C [47] this band was observed for the pyrolysate obtained at 450°C, it gradually loses its intensity at PAC60 and PAC150 with an increase in impregnation ratio pyrolysis temperature which influences the change of substitution of the aromatic rings. All spectra in Fig. 9 also show a broad band in the essential fingerprint spectral region between 1,300 and 900  $\text{cm}^{-1}$  with maxima at 1,080 and 1,165  $\text{cm}^{-1}$ . Usually, the broadband at 1,000–1,300  $\text{cm}^{-1}$  is found in oxidized carbons and assigned to C–O stretching in acids, alcohols, phenols, ethers, and esters [48].

Nevertheless, it also characterizes the phosphorus and the phosphor carbonaceous compounds displayed in the phosphoric acid-activated carbons [49]. Therefore, this band characterizes the P=O bond of ester phosphates; or the O–C bond of P–O–C [50]. Due to the overlap of the absorption bands, assignments in this region are ambitious. In conclusion the IR characterization, the most significant changes introduced by increasing the impregnation ratio of palm tree fibers from 30–150 wt.% are the development of oxygenic groups (band at 1,165 and 3,400  $\text{cm}^{-1}$ ) as well as the increase of phosphorous groups content (band 1,070 and at 1,080  $\text{cm}^{-1}$ ).

### 3.2. Production yield and burn-off

The yield production of activated carbon is higher than that of simple carbonization of the same raw material. As expected, the PACs have higher carbon and ash contents on the other hand have lower oxygen and hydrogen contents compared to the raw material, as found in EDX results (mentioned in Table 3) for the effects of different acid concentrations on the lignocellulosic materials, such

as cellulose, hemicellulose, and lignin. These differences are a primary factor of the activation process [51], by main mechanisms are the depolymerization, dehydration, and redistribution of constituent biopolymers, which leads to the transformation of lignocellulosic materials into carbon, which requires evolving O and H atoms into  $\text{CO}_2$ ,  $\text{CO}$ ,  $\text{H}_2\text{O}$ ,  $\text{CH}_4$ . As a result, it promotes the conversion of aliphatic to aromatic compounds [52], the activation yield and burn-off depend on this carbon. In Table 5, the yield decreases with the increase of the impregnation ratio of 72%, 52%, 40%, and 25% of PAC30, PAC60, PAC100, and PAC150, respectively, which means that the surface area will increase with the development of total porous volume as shown in Table 2. The lower yield of 25% (75% burn-off) was for PAC150. The highest impregnation ratio leads to the enhancement of carbon burning off by excess  $\text{H}_3\text{PO}_4$  widening microporous into mesoporous. It is appropriate to assume that  $\text{P}_2\text{O}_5$  (formed by the dehydration of  $\text{H}_3\text{PO}_4$ ) behaves as an oxidant that can react with the carbon reducing the yield of forming new pores. The “burn-off” of the materials (the activated carbons) increases linearly with the total porous volume and not with the BET surface, confirming that this volume is directly related to mass loss due to activation reactions of the palm fiber trunk (Fig. 10).

### 3.3. Adsorption studies

#### 3.3.1. Sorption isotherms

The adsorption isotherm indicates how the molecules distribute between the liquid and solid phases when the adsorption reaches equilibrium. It is well known that the modeling of adsorption isotherms is the first objective to be achieved in any scientific investigation since it serves as a

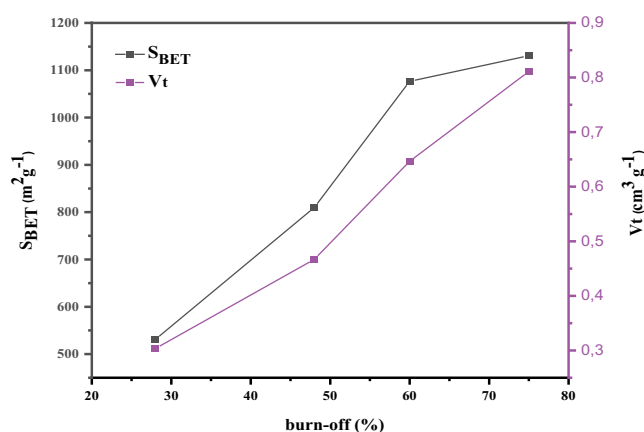


Fig. 10. Evolution of Brunauer–Emmett–Teller surface ( $S_{\text{BET}}$ ) and total porous volume ( $v_s$ ) as a function of “burn-off”.

Table 5

Production yield and burn-off after thermochemical activation of PACs vs. the orthophosphoric acid impregnation ratio

$X_p$ $\text{H}_3\text{PO}_4$ impregnation ratio (wt.%)	PAC30	PAC60	PAC100	PAC150
Production yield of activated carbons (%)	72	52	40	25
Burn-off (or mass loss%)	28	48	60	75

mathematical tool making it possible to pass from the experimental laboratory phase to that of the design on the scale of the prototype. The variation of the amount ( $q_e$ ) of MO dye adsorbed by PACs as a function of the equilibrium concentration ( $C_e$ ) is shown in Fig. 11. On the other hand, several

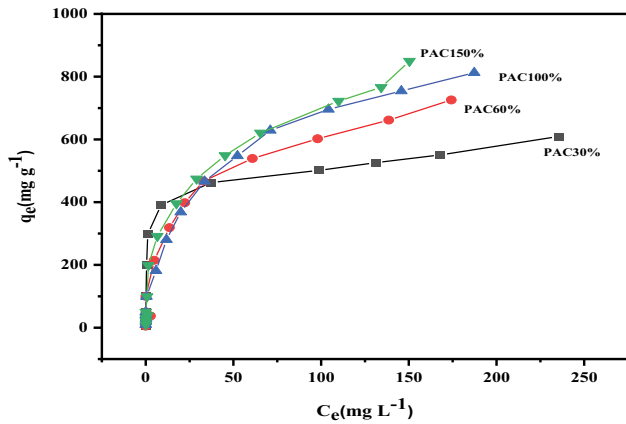


Fig. 11. Adsorption isotherm of methyl orange at pH 4 and 25°C on activated carbons: PAC30, PAC60, PAC100, and PAC150 obtained by phosphoric acid activation of the palm fiber trunk.

models were cited in the literature to describe the experimental data of adsorption isotherms. The Langmuir and Freundlich models are the most frequently used [53].

In this study, these two models, in addition to that of Temkin, are used to describe the interdependence between the amount of adsorbed dye and its equilibrium concentration (Fig. 12). The constants of the isotherms obtained by linearization of the various considered models are summarized in Table 6, while the correlation between the experimental values and those predicted by the best model is illustrated in Fig. 13.

According to Fig. 11, it can be seen that the adsorbed amount at equilibrium ( $q_e$ ) increases with increasing dye concentration ( $C_e$ ), which is consistent with bibliographic data adsorption of MB by activated carbons [13]. Adsorption of 4-chlorophenol by activated carbon prepared from rattan sawdust [53].

As can be seen globally with the shapes of the curves in Fig. 12 and especially the data in Table 6, the Freundlich (Fig. 12a) and Langmuir (Fig. 12b) models are the most appropriate for the four prepared activated carbons with  $R^2$  between 0.9772; 0.9952 and 0.988; 0.9965 for Freundlich and Langmuir models, respectively.

In another way, the Temkin model (Fig. 12c) is the most appropriate only for PAC100 with  $R^2 = 0.99626$ , while the

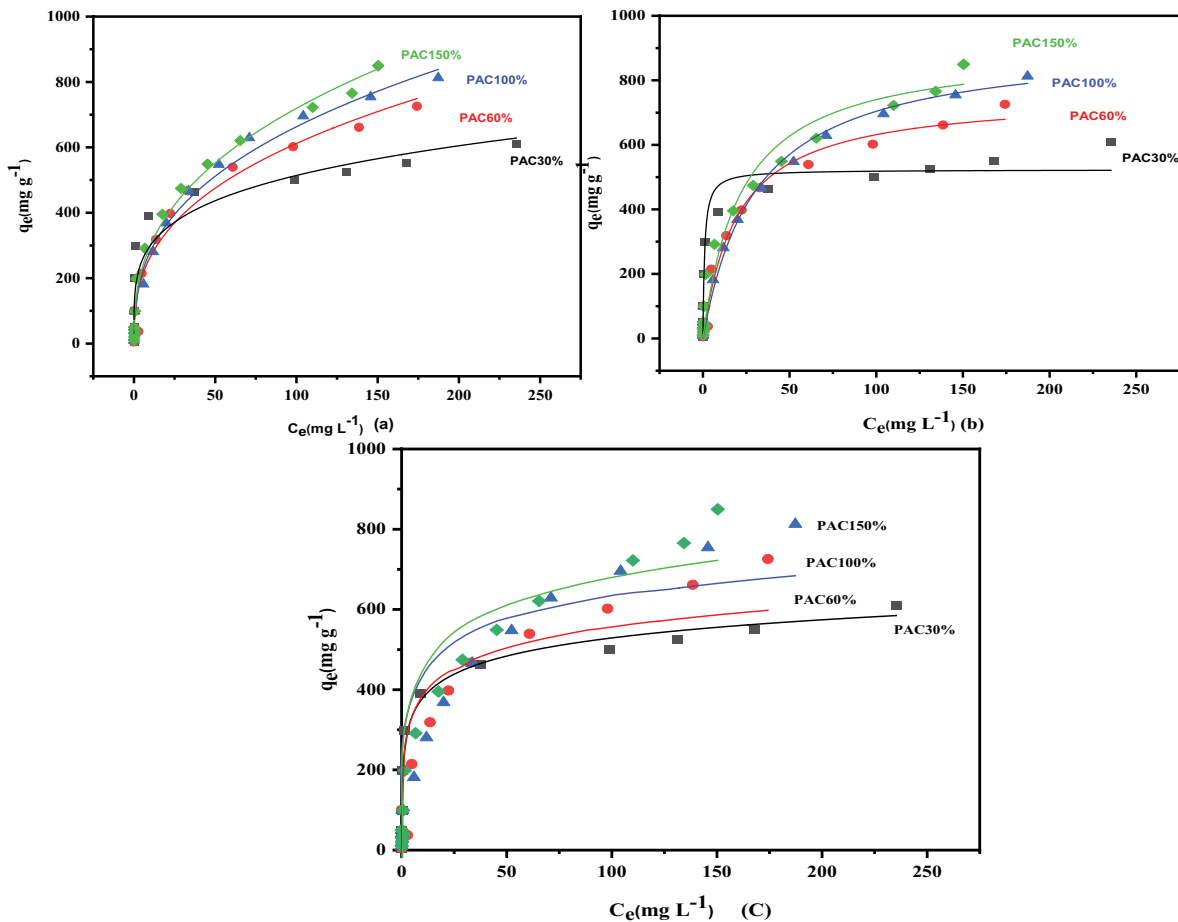


Fig. 12. Experimental adsorption isotherms at pH 4 and 25°C of methyl orange on activated carbons: PAC30, PAC60, PAC100, and PAC150, corresponding Freundlich (a), Langmuir (b) and Temkin (c) models fit (full line).

Table 6  
Langmuir, Freundlich, and Temkin parameters of adsorption isotherms of methyl orange on activated carbons

Activated carbons	Langmuir parameters		$R^2$	Freundlich parameters		$R^2$	Temkin parameters		$R^2$
	$q_m$ (mg·g <sup>-1</sup> )	$K_L$ (L·mg <sup>-1</sup> )		$K_F$ (mg·g <sup>-1</sup> )	$n$		$b_T$ (J·mol <sup>-1</sup> )	$A$ (L·g <sup>-1</sup> )	
PAC30%	578	0.284	0.99	293.08	8.06	0.98	46.504	187.439	0.96
PAC60%	709.219	0.111	0.98	136.11	3.03	0.99	16.363	0.611	0.98
PAC100%	826.446	0.0784	0.97	99.77	2.41	0.98	13.243	0.389	0.99
PAC150%	862	0.0789	0.97	164.88	3.14	0.99	16.99	1.351	0.93

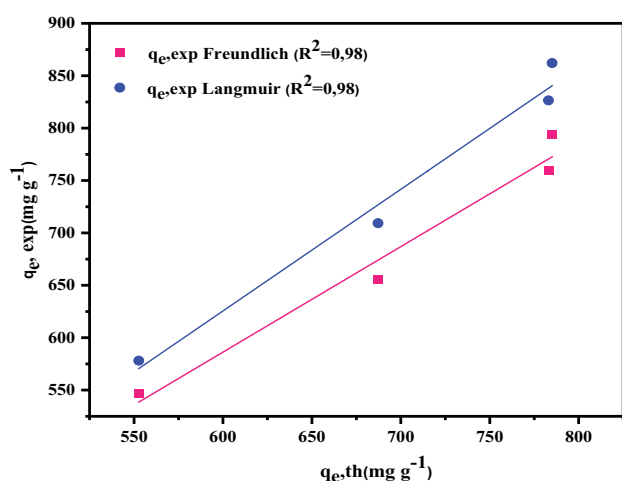


Fig. 13. Correlation between experimental data and those calculated by the Freundlich model for the adsorption of methyl orange at 25°C by activated carbons.

positive constants of the Langmuir model imply the adequacy of this one for the description of the experimental data [54]. Recall that the Freundlich model, of an empirical nature, is used to describe heterogeneous adsorption, while the Langmuir model suggests that the adsorption of molecules takes place on a homogeneous surface in a monolayer without interaction between the adsorbed molecules [53]. However, most of the authors quoted in this document generally find that the adsorption isotherm has an L-type appearance with which the Langmuir model is associated. Concerning the shape of the isotherm and the model type, the results are consistent with those reported by Reffas et al. [13] on the adsorption of Nylosan Red N-2RBL by the activated carbons prepared from coffee grounds by H<sub>3</sub>PO<sub>4</sub> activation. The fit revealed here is supported by the good correlation between ( $q_e$ , experimental) and ( $q_e$ , theory) (Fig. 13).

The adsorption isotherms of MB onto the activated carbons (PACs) are type (I). Fig. 14 suggests that adsorption occurs on specific sites forming a monolayer [55]. The higher the impregnation ratio of PACs, the higher the adsorption capacity ( $q_m$ ) of MB as shown in Table 7. Good agreements of the adsorption isotherms of MB with the Langmuir equations ( $R^2 > 0.99$ ) are found in Table 7. The values of MB amount ( $Q_{MB}$ ) [56] determined from the methylene blue adsorption isotherms are respectively: 349.65, 403.22, 473.93, and 507.61 mg·g<sup>-1</sup> for PAC30, PAC60, PAC100, and PAC150. The amount of MB adsorption of adsorbents increases with

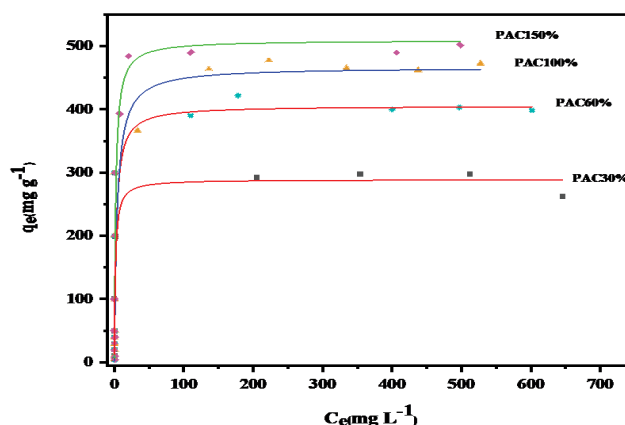


Fig. 14. Experimental adsorption isotherms at pH 6 and 25°C of methylene blue on activated carbons: PAC30, PAC60, PAC100, and PAC150. Langmuir models (full lines).

Table 7  
Langmuir parameters of the adsorption isotherms of methylene blue onto the activated carbons and the surface areas of materials covered by methylene blue molecules

Activated carbon	Parameters of Langmuir		$R^2$
	$q_m$ (mg·g <sup>-1</sup> )	$k_L$ (L·mg <sup>-1</sup> )	
PAC30%	349.65	0.1746	0.998
PAC60%	403.22	0.4275	0.999
PAC100%	473.93	0.2306	0.999
PAC150%	508	0.1461	0.996

an increasing chemical activation ratio [13]. Moreover, the microporous area obtained by the iodine test follows the trend PAC30 > PAC60 > PAC100 > PAC150 and increases with the concentration of phosphoric acid as reported in the literature [57].

### 3.3.2. Discussion of adsorption results

The adsorption also could be explained based on the electrostatic interaction between the ionic dye molecule and the charged activated carbon substrate. At pH 6, where the MB adsorption isotherms were studied, the PAC30, PAC60, and PAC100 activated carbons, are negatively charged ( $\text{pH} > \text{pH}_{\text{PZC}} \sim 5.6$ ) while the PAC150, are positively charged ( $\text{pH} < \text{pH}_{\text{PZC}}$ ). Though electrostatic repulsion between the

MB cation (at pH 6) and PAC150 should not favor adsorption, the highest adsorption uptake is measured for this activated carbon. Thus, the adsorption of MB cannot be controlled only by electrostatic interactions. Indeed, attributed this to the dispersive interactions between the delocalized electrons on the surface of the basic activated carbons and the free conjugated electrons of the dye molecules. Faria et al. [58] and Qian et al. [59] have shown that basic activated carbons still present better performances than acid-activated carbons for the adsorption of cationic dyes.

In the literature, the basicity of activated carbons is described in term of delocalized electrons within the graphene layers, which forms Lewis basic sites (electron donor). Leon y Leon et al. [60] have stated that protons could chemisorb on such sites via electrons carbon pair. The decrease in the electron density on the graphene layers can be predicted to result from the electron-withdrawing effect of carboxylic and lactone groups. Thus, in acidic activated carbons (PAC30, PAC60, and PAC100), a part of the adsorption sites (basal sites) might be shifted from the electron graphene layer to the oxygenated functional groups at the edge of the layers which interact weakly with methylene blue molecules. To conclude, if the porous structure is accessible to MB as in PAC150 (presence of super-microporous and small mesoporous), the slightly basic (almost neutral) the activated carbon, the higher the MB adsorption uptake. The anionic character of MO is due to the presence of a sulfonate group (Table 1), of which the pKa value ( $pK_a = 3.30$ ). The  $pK_a = 3.30$  is determined using two wavelengths  $\lambda = 506.56$  and  $464.5$  nm (Table 1) at pH = 4 the sulfonate group is anionic.

On the contrary pH of PAC30, PAC60, PAC100, and PAC150 are all positively charged ( $pH_{pZC} \sim 5.77, 5.61, 5.58,$  and  $7.22$ , respectively). Thus, the electrostatic attraction is lower for the acidic activated carbons ( $X_p = 30\text{--}100$  wt.%)

than for PAC150 as regards their  $pH_{pZC}$  being  $7.22$ . As a result, the knees of the Langmuir-type adsorption isotherms (Fig. 12a) are pronounced more following these trends: PAC 30 > PAC60 > PAC100 > PAC150, according to the strength of interaction between the activated carbon surface and MO following the decreasing order of the  $pH_{pZC}$  values. The values of the Langmuir constants  $k_L$  reported in Table 6 are in accord with the same trend except for PAC150. As previously mentioned with the MB dye, the adsorption is encore governed by dispersive interactions by the porous volume of the activated carbons, which is accessible to the dye molecule relative to the adsorbent size porous volume of materials. According to its molecular size, this dye can be involved in a sphere with a minimum diameter  $\sim$  of  $1.85$  nm which means that mesoporous is required to adsorb MO.

The MO adsorption capacity is directly proportional to the mesoporous volume, which corresponds to a pore diameter higher than  $\sim 2$  nm (accessible to the MO molecule). This volume can be estimated roughly from the differential pore size distribution (Fig. 6) shows that this appropriate mesoporous volume is larger for PAC150 than for PAC100 and higher for PAC100 than for PAC60. Thus, the activated carbons can be classified by their MO adsorption uptake: PAC150 > PAC100 > PAC60 in agreement with the experimental adsorption results (Fig. 11).

Table 8, represents a comparison of methyl orange and methylene blue adsorption capacity ( $Q_m$ ) by prepared adsorbents with different adsorbents in the literature.

### 3.3.3. Mechanism of the adsorption process

According to surface functional groups which were presented in the method of selective neutralization or Boehm titration and FTIR analysis, porosity measurement by the BJH method,  $pH_{pZC}$ , and the effect of acidic medium on the

Table 8  
Comparison of methyl orange and methylene blue adsorption capacity ( $Q_m$ ) with others adsorbents from the literature

Methyl orange			Methylene blue		
Adsorbent	$Q_m$	References	Adsorbent	$Q_m$	References
Bentonite	118	Bellifa et al. [61]	Sugarcane bagasse	261	Siddiqui et al. [18]
Egusi peeling	13.889	Tchuifon et al. [62]	<i>Moringa oleifera</i> leaf	136.99	Do et al. [63]
Biochar			Biochar		
PAC30	123.1		PAC30	170.06	
PAC60	165	Melouki et al. [64]	PAC60	274.72	Melouki et al. [64]
PAC100	226.7		PAC100	303.03	
PAC150	302.1		PAC150	357.14	
			Globe artichoke leaves		
Waste tyre activated carbon	13.56	Khan et al. [65]	AC1/1	402	Benadjemia et al. [24]
			AC2/1	715	
			AC3/1	599	
Palm trunk fiber			Palm trunk fiber		
PAC30	578		PAC30	349.65	
PAC60	709.21	Present work	PAC60	403.22	Present work
PAC100	826.44		PAC100	473.93	
PAC150	862		PAC150	508	

structure of methyl orange anionic dye, the anionic character of MO is due to the presence of a sulfonate group, of which the  $pK_a$  value ( $pK_a = 3.30$ ). At  $pH = 4$ , the sulfonate group is anionic, the probable adsorption mechanism can be as: At  $pH$  equal 4, the adsorption of methyl orange involves two stages, first the protonation of oxygenated function groups, secondly it followed by three important interactions such as electrostatic attractions between the positively charged functional groups and ( $SO_3^-$ ) of methyl orange,  $\pi$ - $\pi$  interactions,  $\pi$ - $n$  interactions and hydrogen bonds as well as pore filling as illustrated in Fig. 15.

It should be noted that pore filling is not the only mechanism that governs methyl orange dye adsorption by the four activated carbons; other mechanisms may be involved simultaneously in the adsorption process of this system (MO/PACs). FTIR spectra show functional groups that may be involved in the dye adsorption mechanism of methyl orange. Examination of the FTIR spectra of the produced activated carbons shows the appearance of three adsorption bands  $-OH$  ( $-C-OH$ ,  $-COOH$ ),  $C=O$ ,  $C=C$  (confirmed by the Bohem titration) which can be reflected in the existence of interactions between the molecule of methyl orange dye and the active sites of the surface of the activated carbons; these by the shift of the bands, the decrease

and the increase in the intensity of the bands, the disappearance, the duplication of the bands and the decrease in the width at mid-height of the bands after adsorption. The hydroxyl group  $O-H$  enters into the constitution of the hydrogen bond between the methyl orange and the activated carbon surface. Hydrogen bonding occurred between H-donor atoms (i.e., nitrogen) of the acid (anionic) dye molecule and hydroxyl groups (H-acceptors) of the surface of the activated carbons. The aromatic group  $C=C$  intervenes in hydrophobic (a polar) interactions of the  $\pi$ - $\pi$  type (Fig. 15). For anionic dyes, adsorption is governed by interactions between the basic sites on the substrate surface (the  $\pi$  electron acceptor group of the aromatic ring) and the free electrons of the dye molecules (the  $\pi$  electron donor group of the aromatic ring) [66,67]. Regarding carboxylic acid groups; these play the role of electron donor while the aromatic ring of organic compounds (OM) plays the role of electron acceptor. Adsorption is possible through  $n$ - $\pi$  interactions between the electron donor and acceptor. The interaction of MB molecules and the vibrations of chemical functional groups were detected by FTIR analysis of the activated carbons before and after adsorption tests (MB/PACs). At  $pH 6$ , the MB molecule is cationic, the adsorption mechanism can be as: At  $pH$  equal

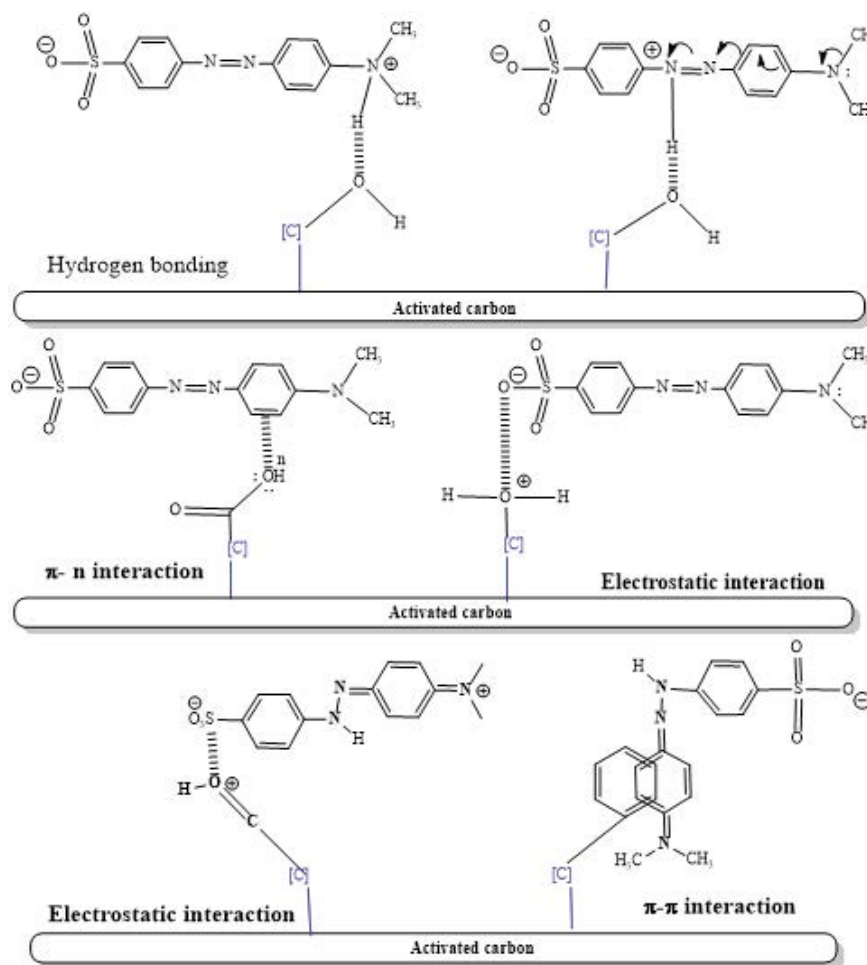


Fig. 15. Probable mechanism of methyl orange adsorption in an acidic medium for PACs.

6 the PAC30, PAC60, and PAC100 activated carbons, are negatively charged ( $\text{pH} > \text{pH}_{\text{PZC}} \sim 5.6$ ) while the PAC150, are positively charged ( $\text{pH} < \text{pH}_{\text{PZC}}$ ). Though electrostatic repulsion between the MB cation (at pH 6) and PAC150 should not favor adsorption, the highest adsorption uptake is measured for this activated carbon. Thus, the adsorption of MB cannot be controlled only by electrostatic interactions. Indeed, attributed this to the dispersive interactions between the delocalized electrons on the surface of the basic activated carbons and the free conjugated electrons of the dye molecules (Fig. 16), these by the shift of the bands, the decrease, the increase of the intensity of the

bands, the disappearance, duplication of the bands and the decrease in the width at half height of the bands after adsorption.

The  $-\text{OH}$  vibration stretches have inferred the occurrence of adsorption as described in various literature [68–70]. After adsorption of MO by activated carbon PAC150, the peaks assigned to  $\text{C}=\text{N}$  and  $\text{C}=\text{C}$  (about  $1,574 \text{ cm}^{-1}$ ) and  $\text{C}-\text{O}$  ( $1,185 \text{ cm}^{-1}$ ) in the activated carbon PAC150 spectrum shifted toward values ( $1,590$  and  $1,164 \text{ cm}^{-1}$ ), suggesting new types of interactions of each of the nitrogen and oxygen functional groups of activated carbon PAC150 in the presence of MO. Indeed, additional peaks were observed in the activated

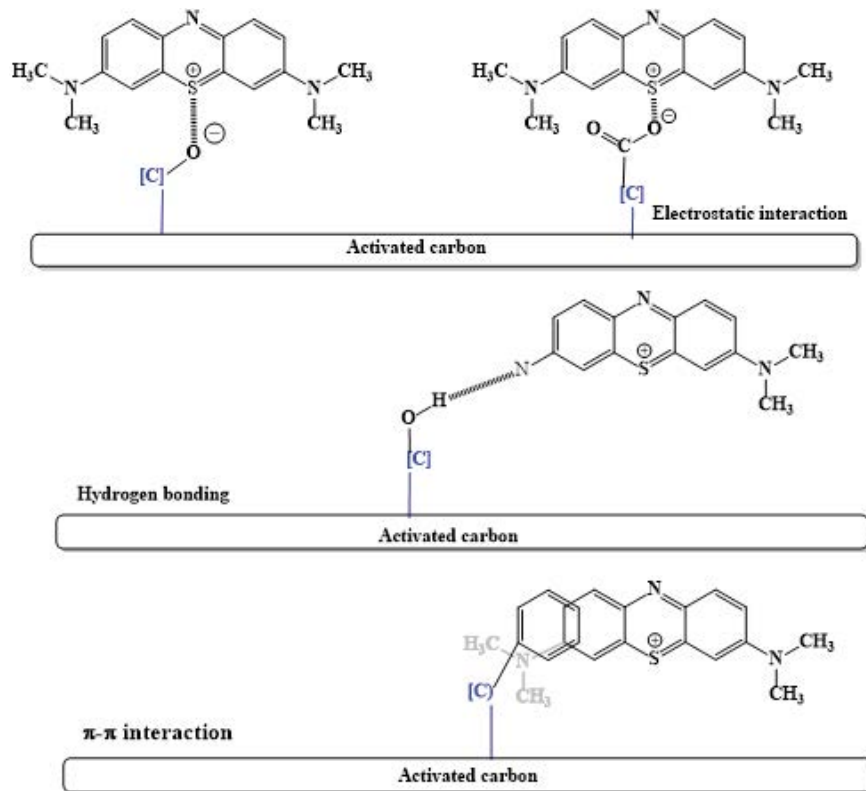


Fig. 16. Probable mechanism of methylene blue adsorption in an acidic medium for PACs.

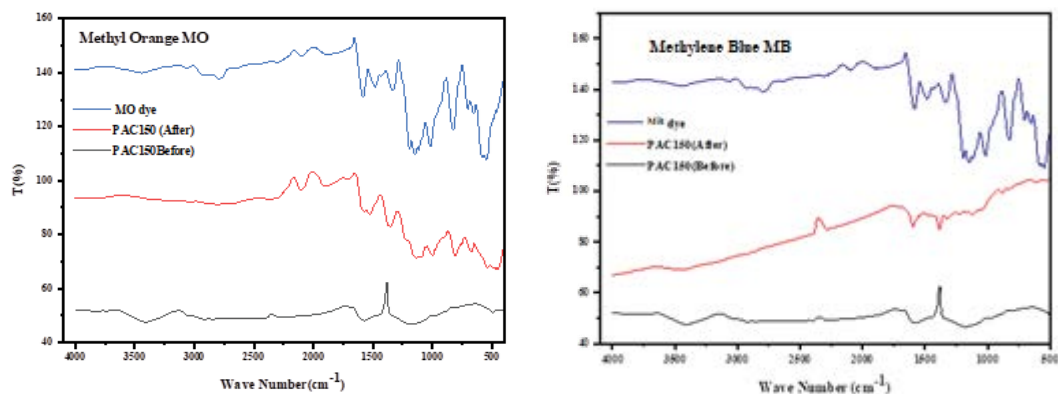


Fig. 17. Fourier-transform infrared spectra of activated carbon PAC150 before and after adsorption of methylene blue and methyl orange.

carbon PAC150-MO spectrum due to the attachment of MO molecules (Fig. 17). The FTIR spectrum of activated carbon PAC150 after MB adsorption showed the peaks of C–O, C=C and O–H bonds at wavenumbers of 1,227; 1,590 and 3,457  $\text{cm}^{-1}$ , respectively. The band at 532  $\text{cm}^{-1}$  was assigned to C–Br, and the band from 719  $\text{cm}^{-1}$  was attributed to C–X (X:F, Cl and/or I) stretching due to the presence of halogen atoms in materials [71,72] and MB. It should be noted that the FTIR curve for the utilized adsorbent with the appearance of peak at wavenumber of 1,320  $\text{cm}^{-1}$  is ascribed to the N–O bond which was absent in the FTIR spectrum of MB [73]. In fact, the peak at a wavenumber of 1,122  $\text{cm}^{-1}$  in spectrum (after adsorption) relates to the C–N stretching from the adsorbed MB molecules (Fig. 17).

#### 4. Conclusion

In this study, activated carbon was prepared from palm trunk fibers by thermoactivation with phosphoric acid. The specific surface area of thermally activated carbon increased after thermochemical activation by phosphoric acid. Therefore, the use of a high impregnation ratio (150%) allows for obtaining exclusively mesoporous carbons with surface areas as high as 1130  $\text{m}^2\cdot\text{g}^{-1}$  and pore volumes as large as 0.81  $\text{cm}^3\cdot\text{g}^{-1}$ .

Due to its high mesoporous content, this latter activated carbon appears as an efficient adsorbent for organic pollutants of molecular size (1.5–3 nm). Therefore, the adsorption equilibrium is accomplished, and the data fit well with the Langmuir, Freundlich, Temkin, and Langmuir models for MO and MB, respectively. The monolayer adsorption capacity of the adsorbent for MB is recognized to be 508  $\text{mg}\cdot\text{g}^{-1}$  and for the MO is more than 862  $\text{mg}\cdot\text{g}^{-1}$  which achieved both Langmuir and Freundlich models. According to the results of adsorption experiments, it can be concluded that PACs are more favorable than most others for azo dyes. This is due to its high surface area, especially in high load ratios as well as diverse porosity.

#### Acknowledgments

The authors express their gratitude to the laboratories of chemistry of the University of Msila, Algeria. And they especially thank Pr. Dakhouch Achour and Dr. Kheniche Abdelhakim for the help and facilities. Also, they thank the section of analysis PTAPC Laghouat for different characterizations.

#### References

- [1] M.F. Hanafi, N. Sapawe, A review on the water problem associate with organic pollutants derived from phenol, methyl orange, and remazol brilliant blue dyes, *Mater. Today Proc.*, 31 (2021) A141–A150.
- [2] N. Ali, A. Said, F. Ali, Z. Ali, F. Raziq, M. Bilal, H.M.N. Iqbal, Photocatalytic degradation of congo red dye from aqueous environment using cobalt ferrite nanostructures: development, characterization, and photocatalytic performance, *Water Air Soil Pollut.*, 231 (2020) 231–250.
- [3] R.J. Mueller, Biological degradation of synthetic polyesters-enzymes as potential catalysts for polyester recycling, *Process Biochem.*, 41 (2006) 2124–2128.
- [4] V.K. Gupta, I. Ali, T.A. Saleh, M.N. Siddiqui, S. Agarwal, Chromium removal from water by activated carbon developed from waste rubber tires, *Environ. Sci. Pollut. Res.*, 20 (2013) 1261–1268.
- [5] Z. Xing, D. Sun, Treatment of antibiotic fermentation wastewater by combined polyferric sulfate coagulation, Fenton and sedimentation process, *J. Hazard. Mater.*, 168 (2009) 1264–1268.
- [6] M.M. Hassan, C.M. Carr, A critical review on recent advancements of the removal of reactive dyes from dyehouse effluent by ion-exchange adsorbents, *Chemosphere*, 209 (2018) 201–219.
- [7] M.N. Khan, O. Bashir, T.A. Khan, S.A. Al-Thabaiti, Z. Khan, CTAB capped synthesis of bio-conjugated silver nanoparticles and their enhanced catalytic activities, *J. Mol. Liq.*, 258 (2017) 133–141.
- [8] M.N. Khan, O. Bashir, T.A. Khan, S.A. Al-Thabaiti, Z. Khan, Catalytic activity of cobalt nanoparticles for dye and 4-nitrophenol degradation: a kinetic and mechanistic study, *Int. J. Chem. Kinet.*, 49 (2017) 438–454.
- [9] R. Dvořák, P. Chlápek, D. Jecha, R. Puchýř, P. Stehlík, New approach to common removal of dioxins and  $\text{NO}_x$  as a contribution to environmental protection, *J. Cleaner Prod.*, 18 (2010) 881–888.
- [10] D.C.K. Ko, V.K.C. Lee, J.F. Porter, G. McKay, Improved design and optimization models for the fixed bed adsorption of acid dye and zinc ions from effluents, *J. Chem. Technol. Biotechnol.*, 77 (2002) 1289–1295.
- [11] W. Thongpat, J. Taweekun, K. Maliwan, Synthesis and characterization of microporous activated carbon from rubberwood by chemical activation with KOH, *Carbon Lett.*, 31 (2021) 1079–1088.
- [12] P. González-García, Activated carbon from lignocellulosics precursors: a review of the synthesis methods, characterization techniques and applications, *Renewable Sustainable Energy Rev.*, 82 (2018) 1393–1414.
- [13] A. Reffas, V. Bernardet, B. David, L. Reinert, M. Bencheikh Lehocine, M. Dubois, N. Batisse, L. Duclaux, Carbons prepared from coffee grounds by  $\text{H}_3\text{PO}_4$  activation: characterization and adsorption of methylene blue and Nylosan Red N-2RBL, *J. Hazard. Mater.*, 175 (2010) 779–788.
- [14] A. El Kassimi, Y. Achour, M. El Himri, M.R. Laamari, M. El Haddad, Process optimization of high surface area activated carbon prepared from *Cucumis melo* by  $\text{H}_3\text{PO}_4$  activation for the removal of cationic and anionic dyes using full factorial design, *Biointerface Res. Appl. Chem.*, 11 (2021) 12662–12679.
- [15] M. Cui, Y. Yu, Y. Zheng, Effective corrosion inhibition of carbon steel in hydrochloric acid by dopamine-produced carbon dots, *Polymers (Basel)*, 13 (2021) 1–16.
- [16] M. Paredes-Laverde, M. Salamanca, J.D. Diaz-Corrales, E. Flórez, J. Silva-Agredo, R.A. Torres-Palma, Understanding the removal of an anionic dye in textile wastewaters by adsorption on  $\text{ZnCl}_2$  activated carbons from rice and coffee husk wastes: a combined experimental and theoretical study, *J. Environ. Chem. Eng.*, 9 (2021) 105685, doi: 10.1016/j.jece.2021.105685.
- [17] T.A. Khan, M. Nouman, D. Dua, S.A. Khan, S.S. Alharthi, Adsorptive scavenging of cationic dyes from aquatic phase by  $\text{H}_3\text{PO}_4$  activated Indian jujube (*Ziziphus mauritiana*) seeds based activated carbon: isotherm, kinetics, and thermodynamic study, *J. Saudi Chem. Soc.*, 26 (2022) 101417, doi: 10.1016/j.jscs.2021.101417.
- [18] M.F. Siddiqui, S.A. Khan, D. Hussain, U. Tabrez, I. Ahmad, T. Fatma, T.A. Khan, A sugarcane bagasse carbon-based composite material to decolor and reduce bacterial loads in waste water from textile industry, *Ind. Crops Prod.*, 176 (2022) 114301, doi: 10.1016/j.indcrop.2021.114301.
- [19] M.V. Lopez-Ramon, F. Stoeckli, C. Moreno-Castilla, F. Carrasco-Marin, On the characterization of acidic and basic surface sites on carbons by various techniques, 37 (1999) 1215–1221.
- [20] J. Jagiello, T. Kyotani, H. Nishihara, Development of a simple NLDFT model for the analysis of adsorption isotherms on zeolite templated carbon (ZTC), *Carbon N. Y.*, 169 (2020) 205–213.

- [21] A. Gómez-Avilés, M. Peñas-Garzón, C. Belver, J.J. Rodríguez, J. Bedia, Equilibrium, kinetics and breakthrough curves of acetaminophen adsorption onto activated carbons from microwave-assisted FeCl<sub>3</sub>-activation of lignin, *Sep. Purif. Technol.*, 278 (2021) 119654, doi: 10.1016/j.seppur.2021.119654.
- [22] N. Abbasi, S.A. Khan, T.A. Khan, Response surface methodology mediated process optimization of Celestine blue B uptake by novel custard apple seeds activated carbon/FeMoO<sub>4</sub> nanocomposite, *J. Water Process Eng.*, 43 (2021) 102267, doi: 10.1016/j.jwpe.2021.102267.
- [23] L. Tschansky, E.R. Graber, Methodological limitations to determining acidic groups at biochar surfaces via the Boehm titration, *Carbon N. Y.*, 66 (2014) 730–733.
- [24] M. Benadjemia, L. Millière, L. Reinert, N. Benderdouche, L. Duclaux, Preparation, characterization and methylene blue adsorption of phosphoric acid activated carbons from globe artichoke leaves, *Fuel Process. Technol.*, 92 (2011) 1203–1212.
- [25] M.A. Al-Ghouti, D.A. Da'ana, Guidelines for the use and interpretation of adsorption isotherm models: a review, *J. Hazard. Mater.*, 393 (2020) 122383, doi: 10.1016/j.jhazmat.2020.122383.
- [26] M. Trachi, N. Bourfis, S. Benamara, H. Gougam, Préparation et caractérisation d'un charbon actif à partir de la coquille d'amande (*Prunus amygdalus*) amère, *Biotechnol. Agron. Soc. Environ.*, 18 (2014) 492–502.
- [27] M.H. Armbruster, J.B. Austin, The adsorption of gases on plane surfaces of mica, *J. Am. Chem. Soc.*, 60 (1938) 467–475.
- [28] H. Freundlich, Über die Adsorption in Lösungen, *Z. Phys. Chem.*, 57 (1907) 385–470.
- [29] F. Kaouah, S. Boumazza, T. Berrama, M. Trari, Z. Bendjama, Preparation and characterization of activated carbon from wild olive cores (oleaster) by H<sub>3</sub>PO<sub>4</sub> for the removal of Basic Red 46, *J. Cleaner Prod.*, 54 (2013) 296–306.
- [30] U. Morali, H. Demiral, S. Şensöz, Optimization of activated carbon production from sunflower seed extracted meal: Taguchi design of experiment approach and analysis of variance, *J. Cleaner Prod.*, 189 (2018) 602–611.
- [31] M. Poletto, H.L. Ornaighi Júnior, A.J. Zattera, Native cellulose: structure, characterization and thermal properties, *Materials (Basel)*, 7 (2014) 6105–6119.
- [32] A. Zubrik, M. Matik, S. Hredzák, M. Lovás, Z. Danková, M. Kováčová, J. Briancin, Preparation of chemically activated carbon from waste biomass by single-stage and two-stage pyrolysis, *J. Cleaner Prod.*, 143 (2017) 643–653.
- [33] G.B. Barin, I. De Fátima Gimenez, L.P. Da Costa, A.G.S. Filho, L.S. Barreto, Influence of hydrothermal carbonization on formation of curved graphite structures obtained from a lignocellulosic precursor, *Carbon N. Y.*, 78 (2014) 609–612.
- [34] Z.C. Kampouraki, D.A. Giannakoudakis, K.S. Triantafyllidis, E.A. Deliyanni, Catalytic oxidative desulfurization of a 4,6-DMDBT containing model fuel by metal-free activated carbons: the key role of surface chemistry, *Green Chem.*, 21 (2019) 6685–6698.
- [35] A. Gutiérrez-Pardo, J. Ramírez-Rico, R. Cabezas-Rodríguez, J. Martínez-Fernández, Effect of catalytic graphitization on the electrochemical behavior of wood derived carbons for use in supercapacitors, *J. Power Sources*, 278 (2015) 18–26.
- [36] W. Kiciński, M. Norek, M. Bystrzejewski, Monolithic porous graphitic carbons obtained through catalytic graphitization of carbon xerogels, *J. Phys. Chem. Solids*, 74 (2013) 101–109.
- [37] M. Sevilla, A.B. Fuertes, Catalytic graphitization of templated mesoporous carbons, *Carbon N. Y.*, 44 (2006) 468–474.
- [38] M. Sevilla, A.B. Fuertes, Graphitic carbon nanostructures from cellulose, *Chem. Phys. Lett.*, 490 (2010) 63–68.
- [39] M. Thommes, Physical adsorption characterization of nanoporous materials, *Chem. Ing. Tech.*, 82 (2010) 1059–1073.
- [40] A.J. Schwanke, S.B.C. Pergher, Porous heterostructured clays - Recent advances and challenges - Revisão, *Cerâmica*, 59 (2013) 576–587.
- [41] E.P. Barrett, L.G. Joyner, P.P. Halenda, The determination of pore volume and area distributions in porous substances. I. Computations from nitrogen isotherms, *J. Am. Chem. Soc.*, 73 (1951) 373–380.
- [42] F. Suárez-García, A. Martínez-Alonso, J.M.D. Tascón, Porous texture of activated carbons prepared by phosphoric acid activation of apple pulp, *Carbon N. Y.*, 39 (2001) 1111–1115.
- [43] M. Jagtoyen, F. Derbyshire, Activated carbons from yellow poplar and white oak by H<sub>3</sub>PO<sub>4</sub> activation, *Carbon N. Y.*, 36 (1998) 1085–1097.
- [44] O. Ioannidou, A. Zabaniotou, Agricultural residues as precursors for activated carbon production—a review, *Renewable Sustainable Energy Rev.*, 11 (2007) 1966–2005.
- [45] E. Yagmur, M. Ozmak, Z. Aktas, A novel method for production of activated carbon from waste tea by chemical activation with microwave energy, *Fuel*, 87 (2008) 3278–3285.
- [46] M.K.B. Gratuito, T. Panyathanmaporn, R.A. Chumnanklang, N. Sirinuntawittaya, A. Dutta, Production of activated carbon from coconut shell: optimization using response surface methodology, *Bioresour. Technol.*, 99 (2008) 4887–4895.
- [47] E. Pehlivan, Production and characterization of activated carbon from pomegranate pulp by phosphoric acid, *J. Turkish Chem. Soc. Chem.*, 5 (2018) 1–8.
- [48] D. Angin, Production and characterization of activated carbon from sour cherry stones by zinc chloride, *Fuel*, 115 (2014) 804–811.
- [49] A. Puziy, O. Poddubnaya, A. Martínez-Alonso, F. Suárez-García, J. Tascón, Synthetic carbons activated with phosphoric acid I. Surface chemistry and ion binding properties, *Carbon*, 40 (2002) 1493–1505.
- [50] A.M. Puziy, O.I. Poddubnaya, A. Martínez-Alonso, F. Suárez-García, J.M.D. Tascón, Surface chemistry of phosphorus-containing carbons of lignocellulosic origin, *Carbon N. Y.*, 43 (2005) 2857–2868.
- [51] S. Yorgun, D. Yildiz, Preparation and characterization of activated carbons from Paulownia wood by chemical activation with H<sub>3</sub>PO<sub>4</sub>, *J. Taiwan Inst. Chem. Eng.*, 53 (2015) 122–131.
- [52] M. Danish, T. Ahmad, A review on utilization of wood biomass as a sustainable precursor for activated carbon production and application, *Renewable Sustainable Energy Rev.*, 87 (2018) 1–21.
- [53] B.H. Hameed, A.L. Ahmad, K.N.A. Latiff, Adsorption of basic dye (methylene blue) onto activated carbon prepared from rattan sawdust, *Dyes Pigm.*, 75 (2007) 143–149.
- [54] B. Uçar, A. Güvenç, Ü. Mehmetoğlu, Use of aluminium hydroxide sludge as adsorbents for the removal of reactive dyes: equilibrium, thermodynamic, and kinetic studies, *J. Waste Water Treat. Anal.*, 2 (2011) 1000112, doi: 10.4172/2157-7587.1000112.
- [55] Y.R. Lin, H. Teng, Mesoporous carbons from waste tire char and their application in wastewater discoloration, *Microporous Mesoporous Mater.*, 54 (2002) 167–174.
- [56] J.C. Santamarina, K.A. Klein, Y.H. Wang, E. Prencsek, Specific surface: determination and relevance, *Can. Geotech. J.*, 39 (2002) 233–241.
- [57] R. Qadeer, S. Akhtar, Kinetics study of lead ion adsorption on active carbon, *Turk. J. Chem.*, 29 (2005) 95–99.
- [58] P.C.C. Faria, J.J.M. Orfão, M.F.R. Pereira, Adsorption of anionic and cationic dyes on activated carbons with different surface chemistries, *Water Res.*, 38 (2004) 2043–2052.
- [59] Q. Qian, M. Machida, H. Tatsumoto, Textural and surface chemical characteristics of activated carbons prepared from cattle manure compost, *Waste Manage.*, 28 (2008) 1064–1071.
- [60] C.A. Leon y Leon, J.M. Solar, V. Calemme, L.R. Radovic, Evidence for the protonation of basal plane sites on carbon, *Carbon N. Y.*, 30 (1992) 797–811.
- [61] A. Bellifa, M. Makhlof, Z.H. Boumila, Comparative study of the adsorption of methyl orange by bentonite and activated carbon, *Acta Phys. Pol. A*, 132 (2017) 466–468.
- [62] D.R. Tchuiwon, S.G. Anagho, E. Njanja, J.N. Ghogomu, N.G. Ndifor-Angwafor, T. Kamgaing, Equilibrium and kinetic modelling of methyl orange adsorption from aqueous solution using rice husk and egussi peeling, *Int. J. Chem. Sci.*, 12 (2014) 741–761.
- [63] T.H. Do, V.T. Nguyen, N.Q. Dung, M.N. Chu, D.V. Kiet, T.T.K. Ngan, L.V. Tan, Study on methylene blue adsorption

- of activated carbon made from *Moringa oleifera* leaf, Mater. Today Proc., 38 (2020) 3405–3413.
- [64] S. Melouki, A. Merrouche, L. Reinert, L. Duclaux, Common reed biochars for the adsorption of methyl orange in aqueous solution, Rev. des Sci. l'Eau., 32 (2020) 349–367.
- [65] T.A. Khan, R. Rahman, E.A. Khan, Adsorption of malachite green and methyl orange onto waste tyre activated carbon using batch and fixed-bed techniques: isotherm and kinetics modeling, Model. Earth Syst. Environ., 3 (2017) 38, doi: 10.1007/s40808-017-0284-1.
- [66] B.K. Pradhan, N.K. Sandle, B.K. Pradhan, Effect of different oxidizing agent treatments on the surface properties of activated carbons, Carbon, 37 (1999) 1323–1332.
- [67] C. Moreno-Castilla, M.V. López-Ramón, F. Carrasco-Marín, Changes in surface chemistry of activated carbons by wet oxidation, Carbon N. Y., 38 (2000) 1995–2001.
- [68] A.H. Jawad, S.H. Mallah, M.S. Mastuli, Adsorption behavior of methylene blue on acid-treated rubber (*Hevea brasiliensis*) leaf, Desal. Water Treat., 124 (2018) 297–307.
- [69] R.A. Rashid, A.H. Jawad, M.A.B.M. Ishak, N.N. Kasim, FeCl<sub>3</sub>-activated carbon developed from coconut leaves: characterization and application for methylene blue removal, Sains Malaysiana, 47 (2018) 603–610.
- [70] A.H. Jawad, R.A. Rashid, M.A.M. Ishak, K. Ismail, Adsorptive removal of methylene blue by chemically treated cellulosic waste banana (*Musa sapientum*) peels, J. Taibah Univ. Sci., 12 (2018) 809–819.
- [71] P.S. Kumar, S. Ramalingam, C. Senthamarai, M. Niranjana, P. Vijayalakshmi, S. Sivanesan, Adsorption of dye from aqueous solution by cashew nut shell: studies on equilibrium isotherm, kinetics and thermodynamics of interactions, Desalination, 261 (2010) 52–60.
- [72] A.A. Spagnoli, D.A. Giannakoudakis, S. Bashkova, Adsorption of methylene blue on cashew nut shell based carbons activated with zinc chloride: the role of surface and structural parameters, J. Mol. Liq., 229 (2017) 65–471.
- [73] P.S. Kumar, S. Ramalingam, K. Sathishkumar, Removal of methylene blue dye from aqueous solution by activated carbon prepared from cashew nut shell as a new low-cost adsorbent, Korean J. Chem. Eng., 28 (2011) 149–155.